

Microseismic data denoising via an apex-shifted hyperbolic Radon transform

Juan I. Sabbione*, Universidad Nacional de La Plata and CONICET, Argentina, and Mauricio D. Sacchi, Department of Physics University of Alberta, Canada and Danilo R. Velis, Universidad Nacional de La Plata and CONICET, Argentina;

SUMMARY

We propose to adopt the apex-shifted hyperbolic Radon transform to improve the signal-to-noise ratio of microseismic records. For this purpose, we design an algorithm that operates in two stages. First, the normalized average envelope of the multicomponent data is transformed to the Radon domain. The coefficients that reconstruct the average envelope are estimated via a threshold criterion. These coefficients are used to define the region of support that is used to denoise individual components by a second application of the apex-shifted hyperbolic Radon transform to individual component gathers.

INTRODUCTION

Hydraulic fracture stimulation and microseismic monitoring are standard processes in nowadays unconventional resources studies (Maxwell, 2011). Although the technique was originally developed to favor the oil production, map the fracture growth, secondary recovery and waste injection operations (Maxwell and Urbancic, 2001), microseismic studies are currently being used for a continuously growing set of applications (Kendall et al., 2011). The standard data processing involves event detection and hypocenter location in order to control fracture dynamics and reservoir development (Eisner et al., 2009). However, over the last years microseismic data are processed to study and analyze additional information such as source mechanisms and fault plane sizes (Baig and Urbancic, 2010; Eisner et al., 2011).

In this work we propose a novel strategy to denoise microseismic data obtained with a single vertical three-components receiver array without using a velocity model. The technique, which is devised to be applied after event detection, can be summarized as follows. First, we consider Michaud and Leaney (2008) ideas and combine the envelope's energy of the three components to obtain an attribute that is independent of the source radiation pattern. Next, we define an apex-shifted hyperbolic operator to represent this attribute in a 4D domain aimed to stack the microseismic signal energy. This representation is posed as an inverse problem, and the inversion is achieved adding a sparsity condition to the cost function and minimizing the misfit. The problem is solved via a Conjugate Gradients method with preconditioning (P-CG) using Iterative Re-weighted Least-Squares (IRLS). This mapping allows us to identify the hyperbola parameters that best represent the microseismic signal (and not the noise) in the transformed domain. Then, a second inversion process is carried out for the x -, y - and z -components separately, but now the inversion is restricted in the transformed domain to the sub-domain identified in the previous stage. Finally, once the data is inverted

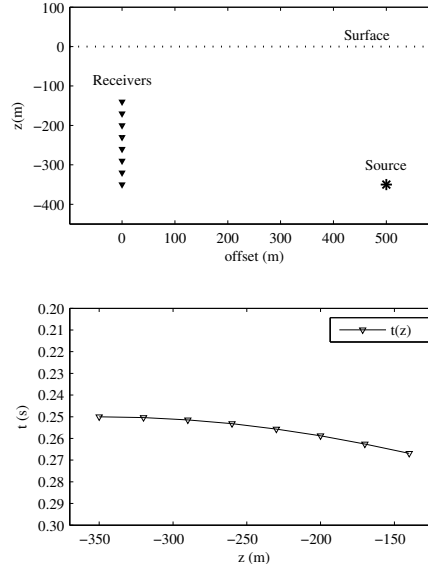


Figure 1: (a) Typical downhole microseismic monitoring survey. (b) Expected arrival times for a constant velocity model.

for each component, we transform back to the data domain thus obtaining the data predicted by the latter inversion. As a consequence, the signal-to-noise of the predicted data is enhanced. The proposed algorithm is illustrated using a synthetic and a field data example. The results show that this inversion technique is very useful to denoise microseismic events signals detected in downhole monitoring.

ALGORITHM DESCRIPTION

Apex-shifted hyperbolic transform

Let us consider a vertical array of receivers deployed in a borehole close to the reservoir and a constant velocity 2D medium as shown in Figure 1a. The arrival time for a seismic event occurring at coordinates (x_s, z_s) is given by

$$t(z) = t_0 + \sqrt{\frac{(x - x_s)^2}{v^2} + \frac{(z - z_s)^2}{v^2}}, \quad (1)$$

where t_0 is the time of the event relative to the origin of the recording time, v is the P or S-wave velocity of the medium and (x, z) indicates the coordinates of the 3-component receiver (Figure 1a).

We can rewrite Equation (1) as follows

$$t(z) = t_0 + \sqrt{t_a^2 + \frac{(z - z_s)^2}{v^2}} \quad (2)$$

Microseismic data denoising

where $t_a = (x - x_s)/v$. Equation (2) represents an apex-shifted hyperbola in the $t - z$ domain with the apex position given by z_s and the time of the apex relative to the origin of the recording time given by $t_0 + t_a$. Thus, using Equation (1) we can map the data into an apex-shifted hyperbolic domain in terms of Radon coefficients that depend on (t_0, x_s, z_s, v) .

Microseismic data are recorded with multicomponent arrays of receivers. The amplitude of the recorded events are affected by the source radiation pattern. If the three-component data are denoted by $d_x(t, z)$, $d_y(t, z)$ and $d_z(t, z)$, we compute the individual envelopes of each component $e_x(t, z)$, $e_y(t, z)$, and $e_z(t, z)$, respectively. After normalization by dividing the envelopes by their maximum, we calculate the average normalized envelope (Michaud and Leaney, 2008):

$$d(t, z) = \frac{1}{3} [e_x(t, z)^2 + e_y(t, z)^2 + e_z(t, z)^2], \quad (3)$$

denoted as $d(t, z)$ to stress that this is our input data to the apex shifted hyperbolic Radon transform. Then we define an adjoint apex-shifted hyperbolic operator (from now the adjoint operator) via the following sum

$$m_a(t_0, x_s, z_s, v) = \sum_{x, z} d(t_0 + \sqrt{\frac{(x - x_s)^2}{v^2} + \frac{(z - z_s)^2}{v^2}}, z). \quad (4)$$

Similarly, the forward apex-shifted hyperbolic operator (from now the forward operator) is defined via

$$d(t, z) = \sum_{x_s, z_s, v} m(t - \sqrt{\frac{(x - x_s)^2}{v^2} + \frac{(z - z_s)^2}{v^2}}, x_s, z_s, v). \quad (5)$$

We now require to devise an algorithm to estimate the coefficients $m(t_0, x_s, z_s, v)$ that represent the data in the transformed domain. One possibility is to use the adjoint operator given by (4) to estimate low resolution coefficients $m_a(t_0, x_s, z_s, v)$. A more convenient approach entails adopting (5) to synthesize $d(t, z)$ in terms of $m(t_0, x_s, z_s, v)$. In other words, we pose the estimation of the transformed domain as an inverse problem (Thorson and Claerbout, 1985). This approach is commonly used in reflection seismology to estimate high-resolution Radon transforms for multiple attenuation.

Let us now switch notation and simplify the problem by adopting the language of linear algebra. The average envelope $d(t, z)$ is organized in a vector \mathbf{d} . Similarly, the Radon coefficients $m(t_0, x_s, z_s, v)$ are also organized into a vector \mathbf{m} . Equation (5) can then be written in matrix form as

$$\mathbf{d} = \mathbf{L}\mathbf{m} + \mathbf{n} \quad (6)$$

where \mathbf{L} represents the forward operator given by Equation (5). Notice that we have also included an additive noise term \mathbf{n} to consider observational errors, inaccuracies that could arise by the constant velocity model approximation and variations of amplitudes. Using a similar argument, Equation (4) can be written as

$$\mathbf{m}_a = \mathbf{L}'\mathbf{d}, \quad (7)$$

where the operator \mathbf{L}' is the adjoint or transpose of \mathbf{L} (Claerbout, 1992). The group of coefficients that represent the data

are estimated by imposing sparsity on the solution \mathbf{m} . The Radon coefficients \mathbf{m} are estimated via the minimization of an l_2 - l_1 cost function

$$\hat{\mathbf{m}} = \underset{\mathbf{m}}{\operatorname{argmin}} [\|\mathbf{L}\mathbf{m} - \mathbf{d}\|_2^2 + \mu\|\mathbf{m}\|_1]. \quad (8)$$

The misfit is minimized to guarantee that the modeled average envelope energy $\mathbf{L}\hat{\mathbf{m}}$ honors the observed data \mathbf{d} . At the same time, we ask the transform domain to be highly focused to facilitate the identification of a microseismic event. The latter is achieved by imposing sparsity on \mathbf{m} through l_1 regularization.

The cost function (8) can be minimized via a variety of methods including Iterative Re-weighted Least-Squares (IRLS) (Scales, 1987; Sacchi and Ulrych, 1995; Daubechies et al., 2010), Iterative Soft-Threshold Algorithm (Figueiredo et al., 2007), etc. In this work, we adopt IRLS with preconditioning to turn minimization of the non-quadratic cost function 8 into the minimization of a sequence of quadratic cost functions via the method of Conjugate Gradients (Hestenes and Stiefel, 1952). This methodology was previously adopted to solve Fourier reconstruction problems by Liu and Sacchi (2004) and least-squares regularized migration by Wang and Sacchi (2007). For this purpose, the non-quadratic regularization term in expression (8) is replaced by

$$\|\mathbf{m}\|_1 \approx \|\mathbf{W}\mathbf{m}\|_2^2, \quad (9)$$

where \mathbf{W} is a diagonal matrix with terms that are given by $W_{ii} = 1/(|m_i| + \epsilon)^{1/2}$ with $\epsilon \ll 1$. We also define a new variable $\mathbf{m} = \mathbf{P}\mathbf{u}$ with diagonal matrix (pre-conditioner) $\mathbf{P} = \mathbf{W}^{-1}$ and solve a sequence of quadratic problems

$$\begin{aligned} \mathbf{u}^k &= \underset{\mathbf{u}}{\operatorname{argmin}} [\|\mathbf{L}\mathbf{P}^{k-1}\mathbf{u} - \mathbf{d}\|_2^2 + \mu\|\mathbf{u}\|_2^2], \quad (10) \\ \mathbf{m}^k &= \mathbf{P}^{k-1}\mathbf{u}^k, \quad k = 1 \dots K, \end{aligned}$$

where k is the iteration number and \mathbf{P}^{k-1} is the matrix of weights computed with \mathbf{m}^{k-1} . The final solution is $\hat{\mathbf{m}} = \mathbf{m}^K$ where K indicates the maximum number of iteration or the iteration at which the algorithm converges. Equation (10) is solved using the Conjugate Gradients method (Hestenes and Stiefel, 1952).

Data denoising

Once we have estimated all the coefficients \mathbf{m} of the apex-shifted hyperbolic transform, we need to select those coefficients that stack the microseismic signal energy. High values of stacked energy can be given either by the P- or the S-wave velocity. As $d(t, z)$ was previously normalized, in an ideal scenario, when stacking exactly over an hyperbolic event, the $m_a(t_0, x_s, z_s, v)$ value obtained by Equation (4) will reach a maximum equal to the number of available channels n_g . Then, we re-scale the inverted coefficients \mathbf{m} with

$$\eta_1 = \max[\mathbf{m}_a] \quad (11)$$

$$\eta_2 = \max[\hat{\mathbf{m}}] \quad (12)$$

$$v = \frac{\eta_1}{\eta_2} \quad (13)$$

so that $(\mathbf{m} = v\hat{\mathbf{m}})$ and now the closer the rescaled radon coefficients are to n_g , the greater the probability that the transform

Microseismic data denoising

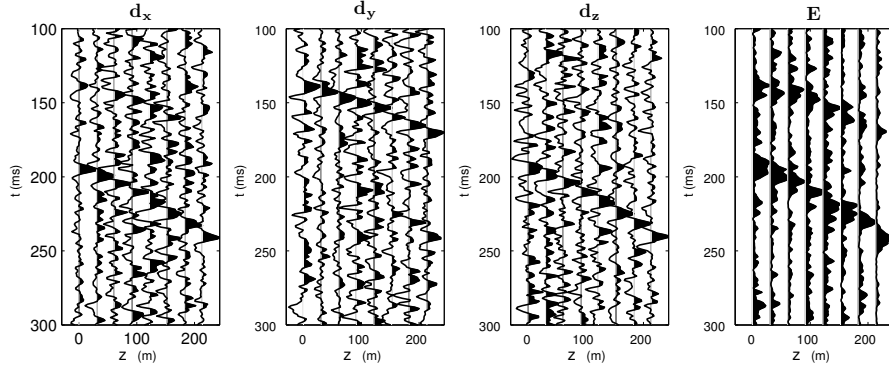


Figure 2: Synthetic dataset example. The x -, y - and z -records (\mathbf{d}_x , \mathbf{d}_y and \mathbf{d}_z , respectively) and the averaged envelope energy used for the first inversion (\mathbf{d}).

is stacking over a microseismic event. To this end, we define a threshold criterion to discern which coefficients correspond to microseismic signal and which do not. We used

$$T = n_g/2 - 1 \quad (14)$$

By this means, we identify the quadruplets (t_0, x_s, z_s, v) that correspond to those $\hat{\mathbf{m}}$ coefficients greater than T and form a subset in the transformed domain. Notice that although the threshold is arbitrary, the final denoising results will not be controlled by T only, but also by the sparsity imposed in the second term of the cost function 8. In other words, the sub-domain determined by T will just help for the sparsity inversion of the data.

The denoised representation of each component is obtained following the same idea. However, we restrict the summation of the forward and adjoint operators (\mathbf{L} and \mathbf{L}^l) to the parameters (t_0, x_s, z_s, v) of that where above threshold. Finally, the three-components noise-attenuated data are calculated transforming back to the time domain using the forward operator \mathbf{L} :

$$\begin{aligned} \hat{\mathbf{d}}_x &= \mathbf{L}\hat{\mathbf{m}}_x \\ \hat{\mathbf{d}}_y &= \mathbf{L}\hat{\mathbf{m}}_y \\ \hat{\mathbf{d}}_z &= \mathbf{L}\hat{\mathbf{m}}_z. \end{aligned} \quad (15)$$

This completes our algorithm description.

SYNTHETIC DATA EXAMPLE

In order to test the proposed algorithm, we generated a synthetic microseismic dataset registered with a 3C vertical array of 8 receivers with the same scheme shown in Figure 1. The 3C clean dataset $u_x(t, z)$, $u_y(t, z)$ and $u_z(t, z)$ was generated by a double-couple source mechanism. Bandpass limited random noise was added to the data so as to obtain the simulated records $d_x(t, z)$, $d_y(t, z)$ and $d_z(t, z)$ with signal-to-noise ratio equal to 1.2. In Figure 2 we show the noise-contaminated synthetic data for each component together with the averaged envelope energy obtained by means of Equation (3). As we have already anticipated, the microseismic signal is barely distinguishable in some channels: try to perceive the S-wave in \mathbf{d}_x ,

or the P-wave in \mathbf{d}_z in Figure 2. Nevertheless, in the envelope panel the microseismic signal energy became clearer as expected, especially for the S-wave, which is less attenuated than the P-wave.

The final results of the proposed technique are shown in Figure 3 against the clean data \mathbf{u}_x , \mathbf{u}_y and \mathbf{u}_z . Although the data was severely contaminated with noise, the waveform and amplitudes of the signal were denoised with a remarkable exactitude in most cases. However, the algorithm exhibits some problems trying to denoise low amplitude signals as those given by the side-lobes of the microseismic wavelet (see Figure 3). This problem is hardly avoided considering two factors: (1) any hyperbola going over low amplitude side-lobes will probably stack not enough energy to satisfy the threshold criterion, and (2) the noise amplitude can totally mask the signal in these cases.

FIELD DATA EXAMPLE

The algorithm was finally tested with a field dataset. Again, the first inversion process was carried out over the averaged envelope energy of the 3C data and the second inversion problem was solved for each component to denoise the data. We show the final results in Figure 4. Of course, the clean data is not available in this case, and the denoised traces are plot against the raw data. The P-wave is below the noise level in this example, and only S-wave arrivals were identified and denoised by the method. Notice that in the z -component the signal-to-noise ratio is good, but it is poor in the x - and y -component, especially for the receivers 1, 2 and 3. Also, the 5th receiver for the x - component exhibits some problem. Nevertheless, the microseismic event was well denoised in most traces and it was also reconstructed by the inversion for the 5th receiver for the x -component.

DISCUSSION

There are some aspects that should be noted and discussed about the proposed denoising approach. We are making a strong

Microseismic data denoising

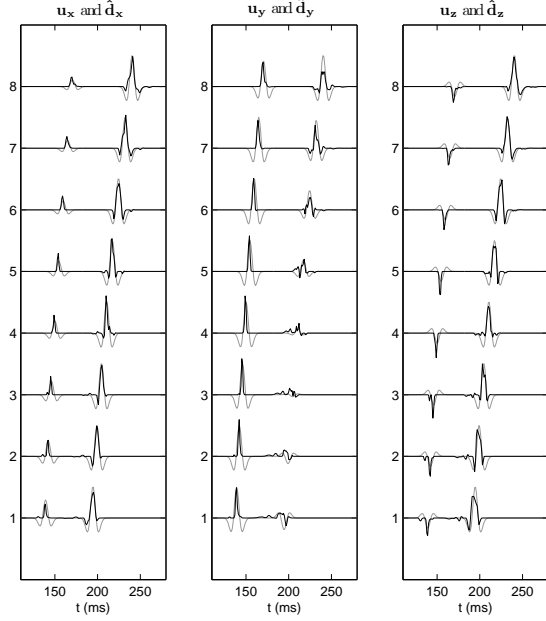


Figure 3: Synthetic data example results. In gray lines the clean synthetic data components (\mathbf{u}_x , \mathbf{u}_y and \mathbf{u}_z) and in black lines the denoised data ($\hat{\mathbf{d}}_x$, $\hat{\mathbf{d}}_y$ and $\hat{\mathbf{d}}_z$).

hypothesis: the velocity model is constant. Although this assumption is not realistic, lets take into account the deviations in the hyperbolic signal arrival that a non-constant velocity model will cause. If these biases are not very large, they are considered in our strategy since a big set of hyperbola parameters (t_0, x_s, z_s, v) are allowed to pass by the threshold criterion. It is worth mentioning that there exist other algorithms devised for microseismic data processing that rely in on a constant velocity model assumption (e.g., (Michaud and Leaney, 2008)).

The proposed denoising algorithm was presented for a 2D model and for a downhole monitoring scenario. However, the method could be extended either for a 3D model or for surface microseismic monitoring data. The main concern about this extension is related to the computational cost that this would require, since the adjoint operator (Equation (4)) will depend on 5 variables (t_0, x_s, y_s, z_s and v) in both cases.

CONCLUSIONS

We devised an algorithm that significantly enhance the signal-to-noise ratio of microseismic events. The denoising is presented as an inverse problem which is solved in two stages. In the first stage, the envelope energies of 3C data are combined and inverted to represent the data in the transformed domain. By means of this representation the parameters that best represent the microseismic arrivals are obtained in the hyperbolic domain. These parameters, together with a sparsity imposition, are used to solve the second inverse problem which is aimed to denoise the data.

The method presented in this paper performed very well de-

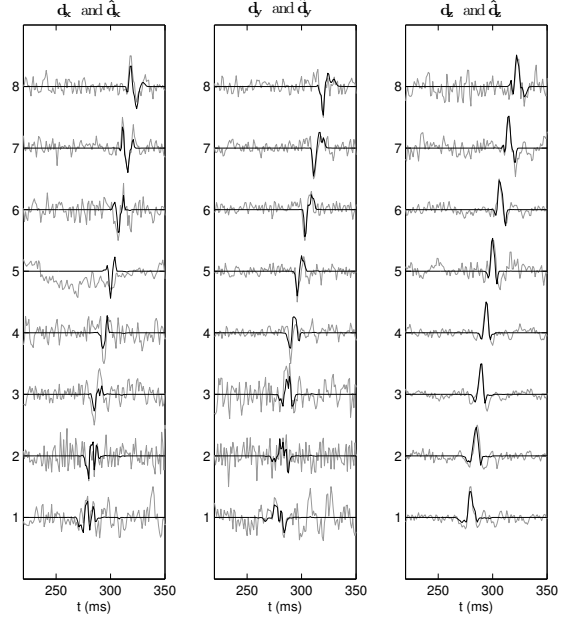


Figure 4: Field data example results. In grey lines the raw data (\mathbf{d}_x , \mathbf{d}_y and \mathbf{d}_z) and in black lines the denoised data ($\hat{\mathbf{d}}_x$, $\hat{\mathbf{d}}_y$ and $\hat{\mathbf{d}}_z$).

noising synthetic data with low signal-to-noise ratio, although some amplitudes where not perfectly recovered. The algorithm could not identified and denoise the P-wave arrivals of the real dataset since the signal was below the noise level. However, the method succeeded reconstructing the microseismic arrival for a single channel that was corrupted by noise. Therefore, we believe this method represents an useful technique to be applied immediately after the event detection when dealing with noisy microseismic data to favor the subsequent data analysis (e.g., hypocenter localization, seismic moment tensor inversion) even when a few channels are corrupted.

ACKNOWLEDGMENTS

This research was supported by the sponsors of the Signal Analysis and Imaging Group (SAIG) at University of Alberta and also by the Consejo Nacional de Investigaciones Científicas y Técnicas (CONICET), Argentina.

Microseismic data denoising

REFERENCES

- Baig, A., and T. Urbancic, 2010, Microseismic moment tensors: A path to understanding frac growth: *The Leading Edge*, **29**, 320–324.
- Claerbout, J., 1992, *Earth soundings analysis: processing versus inversion*: Blackwell Scientific Publications.
- Daubechies, I., R. Devore, M. Fornasier, and C. S. Guentuerk, 2010, Iteratively Reweighted Least Squares Minimization for Sparse Recovery: *Communications on Pure and Applied Mathematics*, **63**, 1–38.
- Eisner, L., P. M. Duncan, W. M. Heigl, and W. R. Keller, 2009, Uncertainties in passive seismic monitoring: *The Leading Edge*, **28**, 648–655.
- Eisner, L., M. P. Thornton, and J. Griffin, 2011, Challenges for microseismic monitoring: SEG, Expanded Abstracts, 1519–1523.
- Figueiredo, M. A. T., R. D. Nowak, and S. J. Wright, 2007, Gradient Projection for Sparse Reconstruction: Application to Compressed Sensing and Other Inverse Problems: *IEEE Journal of Selected Topics in Signal Processing*, **1**, 586–597.
- Hestenes, M., and E. Stiefel, 1952, Methods of conjugate gradients for solving linear systems: *Journal of Research of the National Bureau of Standards*, **49**, 409–436.
- Kendall, M., S. Maxwell, G. Foulger, L. Eisner, and Z. Lawrence, 2011, Special section. Microseismicity: Beyond dots in a box - Introduction: *Geophysics*, **76**, WC1–WC3.
- Liu, B., and M. D. Sacchi, 2004, Minimum weighted norm interpolation of seismic records: *Geophysics*, **69**, 1560–1568.
- Maxwell, S., 2011, What does microseismic tell us about hydraulic fractures?: SEG, Expanded Abstracts, 1565–1569.
- Maxwell, S., and T. Urbancic, 2001, The role of passive microseismic monitoring in the instrumented oil field: *The Leading Edge*, **20**, 636–639.
- Michaud, G., and S. Leaney, 2008, Continuous microseismic mapping for real-time event detection and location: SEG, Expanded Abstracts, **27**, 1357–1361.
- Sacchi, M. D., and T. J. Ulrych, 1995, High-resolution velocity gathers and offset space reconstruction: *Geophysics*, **60**, 1169–1177.
- Scales, J., 1987, Tomographic inversion via the conjugate gradient method: *Geophysics*, **52**, 179.
- Thorson, J. R., and J. F. Claerbout, 1985, Velocity-stack and slant-stack stochastic inversion: *Geophysics*, **50**, 2727–2741.
- Wang, J., and M. D. Sacchi, 2007, High-resolution wave-equation amplitude-variation-with-ray-parameter (AVP) imaging with sparseness constraints: *Geophysics*, **72**, S11–S18.